CrossMark

First Results from BISTRO: A SCUBA-2 Polarimeter Survey of the Gould Belt

Derek Ward-Thompson[1], Kate Pattle[1], Pierre Bastien[2], Ray S. Furuya[3,4], Woojin Kwon[5,6], Shih-Ping Lai[7,8], Keping Qiu[9,10], David Berry[11], Minho Choi[5], Simon Coudé[2], James Di Francesco[12,13], Thiem Hoang[5], Erica Franzmann[14], Per Friberg[11], Sarah F. Graves[11], Jane S. Greaves[15], Martin Houde[16], Doug Johnstone[12,13], Jason M. Kirk[1], Patrick M. Koch[8], Jungmi Kwon[17], Chang Won Lee[5,6], Di Li[18], Brenda C. Matthews[12,13], Joseph C. Mottram[19], Harriet Parsons[11], Andy Pon[16], Ramprasad Rao[8], Mark Rawlings[11], Hiroko Shinnaga[20], Sarah Sadavoy[21], Sven van Loo[22], Yusuke Aso[23,24], Do-Young Byun[5,6], Chakali Eswaraiah[7], Huei-Ru Chen[7,8], Mike C.-Y. Chen[13], Wen Ping Chen[25], Tao-Chung Ching[7,18], Jungyeon Cho[26], Antonio Chrysostomou[27], Eun Jung Chung[5], Yasuo Doi[28], Emily Drabek-Maunder[15], Stewart P. S. Eyres[1], Jason Fiege[14], Rachel K. Friesen[29], Gary Fuller[30], Tim Gledhill[27], Matt J. Griffin[15], Qilao Gu[31], Tetsuo Hasegawa[32], Jennifer Hatchell[33], Saeko S. Hayashi[34], Wayne Holland[35,36], Tsuyoshi Inoue[37,38], Shu-ichiro Inutsuka[38], Kazunari Iwasaki[39], Il-Gyo Jeong[5], Ji-hyun Kang[5], Miju Kang[5], Sung-ju Kang[5], Koji S. Kawabata[40,41,42], Francisca Kemper[8], Gwanjeong Kim[5,6], Jongsoo Kim[5,6], Kee-Tae Kim[5], Kyoung Hee Kim[43], Mi-Ryang Kim[44], Shinyoung Kim[5,6], Kevin M. Lacaille[45], Jeong-Eun Lee[46], Sang-Sung Lee[5,6], Dalei Li[47], Hua-bai Li[31], Hong-Li Liu[18], Junhao Liu[9,10], Sheng-Yuan Liu[8], Tie Liu[5], A-Ran Lyo[5], Steve Mairs[13], Masafumi Matsumura[48], Gerald H. Moriarty-Schieven[12], Fumitaka Nakamura[49,50], Hiroyuki Nakanishi[20,51], Nagayoshi Ohashi[34], Takashi Onaka[23], Nicolas Peretto[15], Tae-Soo Pyo[32,50], Lei Qian[18], Brendan Retter[15], John Richer[52,53], Andrew Rigby[15], Jean-François Robitaille[30], Giorgio Savini[54], Anna M. M. Scaife[30], Archana Soam[5], Motohide Tamura[23,55,56], Ya-Wen Tang[8], Kohji Tomisaka[49,50], Hongchi Wang[57], Jia-Wei Wang[7], Anthony P. Whitworth[15], Hsi-Wei Yen[8,58], Hyunju Yoo[26], Jinghua Yuan[18], Chuan-Peng Zhang[18], Guoyin Zhang[18], Jianjun Zhou[47], Lei Zhu[18], Philippe André[59], C. Darren Dowell[60], Sam Falle[61], and Yusuke Tsukamoto[62]

[1] Jeremiah Horrocks Institute, University of Central Lancashire, Preston PR1 2HE, UK; dward-thompson@uclan.ac.uk, kmpattle@uclan.ac.uk, jmkirk@uclan.ac.uk, spseyres@uclan.ac.uk
[2] Centre de recherche en astrophysique du Québec & département de physique, Université de Montréal, C.P. 6128, Succ. Centre-ville, Montréal, QC, H3C 3J7, Canada; bastien@astro.umontreal.ca, coude@astro.umontreal.ca
[3] Tokushima University, Minami Jousanajima-machi 1-1, Tokushima 770-8502, Japan; rsf@tokushima-u.ac.jp
[4] Institute of Liberal Arts and Sciences Tokushima University, Minami Jousanajima-machi 1-1, Tokushima 770-8502, Japan
[5] Korea Astronomy and Space Science Institute, 776 Daedeokdae-ro, Yuseong-gu, Daejeon 34055, Korea; wkwon@kasi.re.kr, minho@kasi.re.kr, thiemhoang@kasi.re.kr, cwl@kasi.re.kr, bdy@kasi.re.kr, ejchung@kasi.re.kr, igjeong@kasi.re.kr, jkang@kasi.re.kr, mjkang@kasi.re.kr, sjkang@kasi.re.kr, jskim@kasi.re.kr, ktkim@kasi.re.kr, sslee@kasi.re.kr, liutiepku@gmail.com, arl@kasi.re.kr, archana@kasi.re.kr, archer81@kasi.re.kr, syberith@gmail.com
[6] Korea University of Science and Technology, 217 Gajang-ro, Yuseong-gu, Daejeon 34113, Korea
[7] Institute of Astronomy and Department of Physics, National Tsing Hua University, Hsinchu 30013, Taiwan; slai@phys.nthu.edu.tw, eswarbramha@gmail.com, hchen@phys.nthu.edu.tw, chingtaochung@gmail.com
[8] Academia Sinica Institute of Astronomy and Astrophysics, P.O. Box 23-141, Taipei 10617, Taiwan; pmkoch@asiaa.sinica.edu.tw, rrao@asiaa.sinica.edu.tw, ciska@asiaa.sinica.edu.tw, syliu@asiaa.sinica.edu.tw, ywtang@asiaa.sinica.edu.tw, hwyen@asiaa.sinica.edu.tw
[9] School of Astronomy and Space Science, Nanjing University, 163 Xianlin Avenue, Nanjing 210023, China; kpqiu@nju.edu.cn, liujh@smail.nju.edu.cn
[10] Key Laboratory of Modern Astronomy and Astrophysics (Nanjing University), Ministry of Education, Nanjing 210023, China
[11] East Asian Observatory, 660 N. A'ohōkū Place, University Park, Hilo, HI 96720, USA; d.berry@eaobservatory.org, p.friberg@eaobservatory.org, s.graves@eaobservatory.org, h.parsons@eaobservatory.org, m.rawlings@eaobservatory.org
[12] NRC Herzberg Astronomy and Astrophysics, 5071 West Saanich Road, Victoria, BC V9E 2E7, Canada; James.DiFrancesco@nrc-cnrc.gc.ca, douglas.johnstone@nrc-cnrc.gc.ca, brenda.matthews@nrc-cnrc.gc.ca, gerald.schieven@nrc-cnrc.gc.ca
[13] Department of Physics and Astronomy, University of Victoria, Victoria, BC V8P 1A1, Canada; mcychen@uvic.ca, smairs@uvic.ca
[14] Department of Physics and Astronomy, The University of Manitoba, Winnipeg, Manitoba R3T2N2, Canada umfranze@myumanitoba.ca, fiege@physics.umanitoba.ca
[15] School of Physics and Astronomy, Cardiff University, The Parade, Cardiff, CF24 3AA, UK; jane.greaves@astro.cf.ac.uk, e.drabek-maunder@imperial.ac.uk, matt.griffin@astro.cf.ac.uk, nicolas.peretto@astro.cf.ac.uk, br293@exeter.ac.uk, RigbyA@cardiff.ac.uk, anthony.whitworth@astro.cf.ac.uk
[16] Department of Physics and Astronomy, The University of Western Ontario, 1151 Richmond Street, London N6A 3K7, Canada; mhoude2@uwo.ca, apon@uwo.ca
[17] Institute of Space and Astronautical Science, Japan Aerospace Exploration Agency, 3-1-1 Yoshinodai, Chuo-ku, Sagamihara, Kanagawa 252-5210, Japan jungmi.kwon@astron.s.u-tokyo.ac.jp, noonethere94@hotmail.com
[18] National Astronomical Observatories, Chinese Academy of Sciences, A20 Datun Road, Chaoyang District, Beijing 100012, China; ithaca.li@gmail.com, hlliu@nao.cas.cn, lqian@nao.cas.cn, jhyuan@nao.cas.cn, cpzhang@nao.cas.cn, zgyin@nao.cas.cn, lzhupku@gmail.com
[19] Max Planck Institute for Astronomy, Königstuhl 17, D-69117 Heidelberg, Germany; mottram@mpia.de
[20] Kagoshima University, 1-21-35 Korimoto, Kagoshima, Kagoshima 890-0065, Japan; shinnaga@sci.kagoshima-u.ac.jp, hnakanis@sci.kagoshima-u.ac.jp
[21] Harvard-Smithsonian Center for Astrophysics, 60 Garden Street, Cambridge, MA 02138, USA; sarah.sadavoy@cfa.harvard.edu
[22] School of Physics and Astronomy, University of Leeds, Woodhouse Lane, Leeds LS2 9JT, UK; physvl@leeds.ac.uk
[23] The University of Tokyo, 7-3-1 Hongo, Bunkyo-ku, Tokyo 113-0033, Japan; yusuke@naoj.org, onaka@astron.s.u-tokyo.ac.jp, motohide.tamura@nao.ac.jp
[24] Department of Astronomy, Graduate School of Science, University of Tokyo, 7-3-1 Hongo, Bunkyo-ku, Tokyo 113-0033, Japan
[25] Institute of Astronomy, National Central University, Chung-Li 32054, Taiwan; wchen@gm.astro.ncu.edu.tw
[26] Department of Astronomy and Space Science, Chungnam National University, 99 Daehak-ro, Yuseong-gu, Daejeon 34134, Korea; jcho@cnu.ac.kr, hyunju527@gmail.com
[27] School of Physics, Astronomy & Mathematics, University of Hertfordshire, College Lane, Hatfield, Hertfordshire AL10 9AB, UK; a.chrysostomou@herts.ac.uk, t.gledhill@herts.ac.uk
[28] The University of Tokyo, 3-8-1 Komaba, Meguro, Tokyo 153-8902, Japan; doi@ea.c.u-tokyo.ac.jp
[29] Dunlap Institute for Astronomy & Astrophysics, University of Toronto, Toronto, Ontario M5S 3H4, Canada; friesen@dunlap.utoronto.ca
[30] Jodrell Bank Centre for Astrophysics, School of Physics and Astronomy, University of Manchester, Oxford Road, Manchester, M13 9PL, UK; G.Fuller@manchester.ac.uk, jean-francois.robitaille@manchester.ac.uk, anna.scaife@manchester.ac.uk
[31] Department of Physics, The Chinese University of Hong Kong, Shatin, N.T., Hong Kong; qlgu@phy.cuhk.edu.cn, hbli@phy.cuhk.edu.hk
[32] National Astronomical Observatory, National Institutes of Natural Sciences, Osawa, Mitaka, Tokyo 181-8588, Japan; tetsuo.hasegawa@nao.ac.jp, pyo@naoj.org
[33] Physics and Astronomy, University of Exeter, Stocker Road, Exeter EX4 4QL, UK; hatchell@astro.ex.ac.uk
[34] National Astronomical Observatory of Japan, 650 N. A'ohōkū Place, Hilo, HI 96720, USA; saeko@naoj.org, nohashi@naoj.org

[35] UK Astronomy Technology Centre, Royal Observatory, Blackford Hill, Edinburgh EH9 3HJ, UK; wayne.holland@stfc.ac.uk
[36] Institute for Astronomy, University of Edinburgh, Royal Observatory, Blackford Hill, Edinburgh EH9 3HJ, UK
[37] Nagoya University, Furo-cho, Chikusa-ku, Nagoya 464-8602, Japan; tsuyoshi.inoue@nao.ac.jp
[38] Department of Physics, Graduate School of Science, Nagoya University, Furo-cho, Chikusa-ku, Nagoya 464-8602, Japan; inutsuka@nagoya-u.jp
[39] Department of Environmental Systems Science, Doshisha University, Tatara, Miyakodani 1-3, Kyotanabe, Kyoto 610-0394, Japan; kiwasaki@mail.doshisha.ac.jp
[40] Hiroshima Astrophysical Science Center, Hiroshima University, Kagamiyama 1-3-1, Higashi-Hiroshima, Hiroshima 739-8526, Japan; kawabtkj@hiroshima-u.ac.jp
[41] Department of Physics, Hiroshima University, Kagamiyama 1-3-1, Higashi-Hiroshima, Hiroshima 739-8526, Japan
[42] Core Research for Energetic Universe (CORE-U), Hiroshima University, Kagamiyama 1-3-1, Higashi-Hiroshima, Hiroshima 739-8526, Japan
[43] Department of Earth Science Education, Kongju National University, 56 Gongjudaehak-ro, Gongju-si 32588, Korea; quarkosmos@kasi.re.kr
[44] Department of Physics, Institute for Astrophysics, Chungbuk National University, Korea; koon7680@gmail.com
[45] Department of Physics and Atmospheric Science, Dalhousie University, Halifax B3H 4R2, Canada; kevinlacaille@dal.ca
[46] School of Space Research, Kyung Hee University, 1732 Deogyeong-daero, Giheung-gu, Yongin-si, Gyeonggi-do 17104, Korea; jeongeun.lee@khu.ac.kr
[47] Xinjiang Astronomical Observatory, Chinese Academy of Sciences, 150 Science 1-Street, Urumqi 830011, Xinjiang, China; lidalei@xao.ac.cn, zhoujj@xao.ac.cn
[48] Kagawa University, Saiwai-cho 1-1, Takamatsu, Kagawa, 760-8522, Japan; matsu@ed.kagawa-u.ac.jp
[49] Division of Theoretical Astronomy, National Astronomical Observatory of Japan, Mitaka, Tokyo 181-8588, Japan
fumitaka.nakamura@nao.ac.jp, tomisaka@th.nao.ac.jp
[50] SOKENDAI (The Graduate University for Advanced Studies), Hayama, Kanagawa 240-0193, Japan
[51] Japan Aerospace Exploration Agency, 3-1-1, Yoshinodai, Chuo-ku, Sagamihara, Kanagawa 252-5210, Japan
[52] Astrophysics Group, Cavendish Laboratory, J J Thomson Avenue, Cambridge CB3 0HE, UK; jsr10@cam.ac.uk
[53] Kavli Institute for Cosmology, Institute of Astronomy, University of Cambridge, Madingley Road, Cambridge, CB3 0HA, UK
[54] OSL, Physics & Astronomy Dept., University College London, WC1E 6BT London, UK; g.savini@ucl.ac.uk
[55] Astrobiology Center of NINS, 2-21-1 Osawa, Mitaka, Tokyo 181-8588, Japan
[56] National Astronomical Observatory of Japan, NINS, 2-21-1, Osawa, Mitaka, Tokyo, 181-8588, Japan
[57] Purple Mountain Observatory, Chinese Academy of Sciences, 2 West Beijing Road, 210008 Nanjing, PR China; hcwang@pmo.ac.cn
[58] European Southern Observatory (ESO), Karl-Schwarzschild-Straße 2, D-85748 Garching, Germany
[59] Laboratoire AIM CEA/DSM-CNRS-Université Paris Diderot, IRFU/Service dAstrophysique, CEA Saclay, F-91191 Gif-sur-Yvette, France; philippe.andre@cea.fr
[60] Jet Propulsion Laboratory, M/S 169-506, 4800 Oak Grove Drive, Pasadena, CA 91109, USA; cdd@astro.caltech.edu
[61] Department of Applied Mathematics, University of Leeds, Woodhouse Lane, Leeds LS2 9JT, UK; S.A.E.G.Falle@leeds.ac.uk
[62] RIKEN, 2-1 Hirosawa, Wako, Saitama 351-0198, Japan; yusuke.tsukamoto@riken.jp

Abstract

We present the first results from the B-fields In STar-forming Region Observations (BISTRO) survey, using the Sub-millimetre Common-User Bolometer Array 2 camera, with its associated polarimeter (POL-2), on the James Clerk Maxwell Telescope in Hawaii. We discuss the survey's aims and objectives. We describe the rationale behind the survey, and the questions that the survey will aim to answer. The most important of these is the role of magnetic fields in the star formation process on the scale of individual filaments and cores in dense regions. We describe the data acquisition and reduction processes for POL-2, demonstrating both repeatability and consistency with previous data. We present a first-look analysis of the first results from the BISTRO survey in the OMC 1 region. We see that the magnetic field lies approximately perpendicular to the famous "integral filament" in the densest regions of that filament. Furthermore, we see an "hourglass" magnetic field morphology extending beyond the densest region of the integral filament into the less-dense surrounding material, and discuss possible causes for this. We also discuss the more complex morphology seen along the Orion Bar region. We examine the morphology of the field along the lower-density northeastern filament. We find consistency with previous theoretical models that predict magnetic fields lying parallel to low-density, non-self-gravitating filaments, and perpendicular to higher-density, self-gravitating filaments.

Key words: ISM: individual objects (Orion A, OMC1) – polarization – stars: formation – stars: magnetic field – submillimeter: ISM

1. Introduction

Our knowledge of the star formation process has increased dramatically as a result of the advent of satellites such as *Spitzer* and *Herschel*, and sensitive far-infrared and submillimeter detector arrays such as the Sub-millimetre Common-User Bolometer Array 2 (SCUBA-2). Following on from the highly successful first-generation James Clerk Maxwell Telescope (JCMT) Legacy Surveys, including the Gould Belt Legacy Survey (e.g., Ward-Thompson et al. 2007, 2016; Buckle et al. 2010; Graves et al. 2010; Sadavoy et al. 2013; Pattle et al. 2015, 2017; Rumble et al. 2015; Salji et al. 2015; Chen et al. 2016; Kirk et al. 2016; Mairs et al. 2016), the JCMT is currently undertaking a series of second-generation surveys, using the latest instruments to be commissioned on the telescope. These include POL-2, an imaging polarimeter for SCUBA-2. One of the surveys using POL-2 is the B-fields in STar-forming Region Observations (BISTRO) Survey that we report here. This is extremely timely because magnetic fields (hereafter referred to as B-fields) are still not well understood in star formation because of a paucity of observational evidence, despite widespread theoretical recognition of the significance of B-fields in the formation of cores (e.g., Basu et al. 2009 and references therein) and the evolution of protostars (e.g., Li et al. 2011 and references therein).

1.1. Observing Magnetic Fields

The submillimeter continuum emission from dust grains is polarized because the grains tend toward alignment perpendicular to B-field lines. For asymmetric particles with some ability to be magnetized, a series of relaxation processes brings the grains toward their lowest energy rotation state. This is with the longest axis perpendicular to the field (Lazarian & Hoang 2008).

Hence, with material along this axis contributing more to the total far-infrared/submillimeter grain emission, linear

polarization is seen perpendicular to the field. In the grain alignment process, the radiative torque that spins up irregularly shaped grains is thought to play the most significant role (e.g., Lazarian & Hoang 2008). A few percent polarization is detected astronomically, on scales from protostars and jets, up to giant molecular clouds. In some completely symmetric geometries the field lines cancel out so that there is a polarization null. Nevertheless, submillimeter continuum polarization surveys represent a powerful technique for tracing the plane-of-sky B-field orientation (e.g., Matthews et al. 2009; Dotson et al. 2010).

The fractional polarization from dust yields no direct estimate of the B-field strength, since it is dependent on several additional unknowns (e.g., efficiency of grain alignment, grain shape, and composition). However, a measure of the field strength can be derived from the commonly used Chandrasekhar-Fermi (C-F) method (Chandrasekhar & Fermi 1953), and modern variants thereof (e.g., Hildebrand et al. 2009; Houde et al. 2009), using dispersion in polarization half-vectors (where high dispersion indicates a highly turbulent velocity field and a weak mean B-field component; "half-vector" refers to the ±180° ambiguity in B-field direction), the line widths estimated from spectroscopic data, and the density from the SCUBA-2 flux densities (e.g., Crutcher et al. 2004; Kirk et al. 2006). Simulations show that this estimate can be corrected for a statistical ensemble of objects to yield realistic estimates of the field strength (Heitsch et al. 2001; Ostriker et al. 2001; Falceta-Gonçalves et al. 2008). In addition, the effects of multiple eddies along the line of sight have been studied by Cho & Yoo (2016).

B-field geometries are generally inferred by preferential emission or absorption by dust or molecules, creating polarized light (e.g., Houde et al. 2004, 2013; Cho & Lazarian 2007). Polarization measurements with molecules require bright lines and are generally restricted to very dense small-scale structures. Near-infrared absorption polarimetry requires a large sample of background stars and is generally limited to more diffuse cloud material of lower density (Goodman et al. 1990; see also Kwon et al. 2015; Tamura & Kwon 2015).

B-field strengths are typically measured using Zeeman splitting of paramagnetic molecules (e.g., Crutcher et al. 2010). While detections of Zeeman splitting in the high-density tracer CN have been made toward extremely bright sources (e.g., Crutcher et al. 1996), Zeeman splitting measurements are typically restricted to lower-density regions of molecular clouds, where the OH molecule is relatively highly abundant (e.g., Troland & Crutcher 2008).

In contrast, polarized far-infrared and submillimeter thermal dust emission can trace dense structures on both cloud scales and core scales. The *Planck* satellite has generated an all-sky submillimeter polarization map (Planck Collaboration et al. 2015), allowing us to trace the large-scale B-field over the entire sky. However, it is at too low resolution (∼4 arcmin at 857 GHz; Planck HFI Core Team 2011) to study the detailed cloud geometries in star-forming regions on the necessary scale of prestellar cores and protostars. At somewhat better resolution (30 arcsec at 250 μm; Pascale et al. 2008), the BLASTPol balloon-borne polarimeter has mapped a limited number of star-forming regions in great detail (e.g., Matthews et al. 2014; Fissel 2015; Fissel et al. 2016).

1.2. Theoretical Models

The theoretical role played by B-fields in star formation has been much discussed (e.g., Mouschovias 1991; Padoan & Nordlund 1999; Mac Low & Klessen 2004; Nakamura & Li 2005; Vázquez-Semadeni et al. 2011; Inutsuka et al. 2015). However, systematic surveys to measure B-fields in star-forming regions on the necessary resolution scales have proved problematic (see recent reviews by Crutcher 2012; Li et al. 2014). POL-2 with SCUBA-2 on JCMT is a facility that can map the B-field within cold dense cores and filaments on scales of ∼1000–2000 au in nearby star-forming regions, such as those in the Gould Belt. As such, it can provide a link between the B-field measured on arcminute scales by Planck (Planck Collaboration et al. 2015) and BLASTPol (e.g., Matthews et al. 2014) with measurements made on arcsecond scales by interferometers such as the Submillimeter Array (SMA; e.g., Girart et al. 2006; Tang et al. 2010; Chen et al. 2012), Combined Array for Research in Millimeter-wave Astronomy (CARMA; e.g., Hull et al. 2013, 2014), and the Atacama Large Millimeter/submillimeter Array (ALMA; e.g., Cortes et al. 2016; Nagai et al. 2016). This intermediate-size scale is crucial to testing theoretical models of star formation.

As a result of observations made by the *Herschel* satellite, it is now widely believed that most low-mass stars form according to the so-called filamentary star formation model (André et al. 2014). This model has been debated for some time. However, *Herschel* has shown that this appears to be the dominant star-forming mechanism for solar-type stars (André et al. 2014). In this scenario a cloud first breaks up into filaments, and material flows onto the filaments along striations, or subfilaments (e.g., Palmeirim et al. 2013). A similar picture of movement of material along filaments was previously observed and inferred from a combination of spectroscopic data and simulations (e.g., Balsara et al. 2001 —using data from Richer et al. 1993). However, this was just one region. *Herschel* appears to show the same mechanism in many star-forming regions.

In this model the B-field aligns with the striations (i.e., perpendicular to the filaments), and helps to "funnel" matter onto the filaments. This observationally informed paradigm has been reproduced by recent simulations of magnetized self-gravitating filaments (e.g., Inoue & Inutsuka 2008, 2009, 2012; Li et al. 2010; Soler et al. 2013). Cores then form on filaments, becoming gravitationally unstable and subsequently collapsing to form protostars (André et al. 2014).

We know from large-scale polarization studies, e.g., Planck and BLASTPol amongst others (see above), that large-scale fields typically lie roughly perpendicular to their associated filament direction (e.g., Sugitani et al. 2011; Palmeirim et al. 2013; Matthews et al. 2014; Planck Collaboration et al. 2015), but we do not know what happens to the field within the dense gas of the filaments themselves, nor what happens within the cores that form in the filaments (see BLASTPol; Matthews et al. 2014). This is crucial to understanding the physical processes taking place, and to discriminating between the models of the star formation process that properly incorporate B-fields (e.g., Nakamura & Li 2005; Vázquez-Semadeni et al. 2011; Seifried & Walch 2015).

The current hypotheses are that the field may wrap around the filament in a helical manner (e.g., Shibata & Matsumoto 1991; Fiege & Pudritz 2000a); turn to run parallel to the filament in the

densest gas (e.g., the purely poloidal field model of Fiege & Pudritz 2000b); or take on a pinched morphology perpendicular to the long axis of the filament (e.g., Tomisaka 2015; Burge et al. 2016), similar to that produced in initially magnetically supported cores in the classical ambipolar-diffusion paradigm (e.g., Galli & Shu 1993; Crutcher et al. 2004).

Theoretical studies have shown that both B-fields (e.g., Li & Nakamura 2004; Basu et al. 2009) and turbulence (e.g., Klessen et al. 2000; Heitsch et al. 2011) can significantly affect how dense structures form, collapse, and evolve in the interstellar medium. For example, one paradigm of low-mass star formation suggests that collapse is guided by B-fields, producing flattened cores and disks (e.g., Mouschovias 1991). This collapse (and subsequent protostar formation) can drag and twist the field lines, amplifying the local field strength during the early stages of protostellar evolution (e.g., Machida et al. 2005; Hennebelle & Teyssier 2008; Li et al. 2011). These twisted lines can then have significant consequences for the emerging protostellar outflows, disks, frequency of binarity, and stellar masses (e.g., Price & Bate 2007; Hennebelle & Fromang 2008; Machida et al. 2011).

In fact, there is a debate about the relative importance of B-fields and turbulence in regulating the star formation process (e.g., Mouschovias 1991; Padoan & Nordlund 2002). The POL-2 observations, combined with our existing kinematics from HARP-B (e.g., Buckle et al. 2010), will allow for an investigation into the balance between gravity, turbulent support, and B-fields over a statistically meaningful number of star-forming cores in a number of regions across the Gould Belt.

Once protostars have formed, there is also a debate about the role that the B-field plays in shaping protostellar evolution and its effect on bipolar outflows. For example, recent studies on the correlation of B-field direction with outflows, using CARMA polarization observations, found no correlation between outflow and field directions on scales below 1000 au (Hull et al. 2014).

In contrast, a large-scale correlation between outflow and field directions has been found on scales of ~10,000 au and above (Chapman et al. 2013). One explanation of this apparent conflict in the field morphology uses detailed modeling of toroidally wrapped B-fields at the centers of clouds (Segura-Cox et al. 2015). This has been used to explain early disk formation in Class 0 protostars in a recent model in which early disks are hypothesized to preferentially be formed in fields misaligned with the outflow directions (Segura-Cox et al. 2015). POL-2 data are crucial to filling in the missing information on intermediate scales between ~1000 and ~10,000 au. The BISTRO survey aims to address this and all of the other questions discussed above.

Previously, only a few prestellar and protostellar cores have had their B-fields mapped (e.g., Holland et al. 1999; Ward-Thompson et al. 2000, 2009; Matthews & Wilson 2002; Crutcher et al. 2004; Kirk et al. 2006). BISTRO will map hundreds. In this paper we describe the plan for the BISTRO survey and discuss the first results taken on OMC 1.

2. Aims and Objectives of the Survey

Previous surveys have either been piecemeal, been very restricted in sample size (e.g., Matthews et al. 2009; Vaillancourt & Matthews 2012; Hull et al. 2013, 2014; Matthews et al. 2014), or have too poor resolution to detect cores and protostars (e.g.,

Planck Collaboration et al. 2015). We here describe a project that aims to produce a large and unbiased survey of the B-fields in star-forming molecular material in the solar vicinity, simultaneously at 850 and 450 μm, and at relatively high resolution—14.1 and 9.6 arcsec, respectively (Dempsey et al. 2013), or ~1000–2000 au at a typical Gould Belt cloud distance.

The BISTRO Survey is a large-scale survey of the Gould Belt clouds that we have previously mapped in continuum and spectral lines at JCMT (e.g., Ward-Thompson et al. 2007; Buckle et al. 2015; White et al. 2015), and in the far-infrared with *Herschel* (André et al. 2010).

The aims of the project are to obtain maps of polarization position angle and fractional polarization in a statistically meaningful sample of cores in numerous regions; to characterize the evidence for and relevance of the B-field and turbulence (in conjunction with previous and follow-up spectroscopic line observations) in cores and their surrounding environments; to test the predictions of low-mass star formation theories (core, filament, outflow, and field geometry) and grain alignment theories; to generate a large sample of objects that are suitable for follow-up with other instruments, such as ALMA, Nobeyama, SMA, and NOEMA (NOrthern Extended Millimeter Array); and to measure the B-field strength using the C-F method in as many clouds as possible within our sample.

The survey was granted an initial allocation of 224 hr of telescope time to observe 16 fields in 7 different Gould Belt clouds (Auriga, IC5146, Ophiuchus, Orion, Perseus, Serpens, and Taurus). The specific fields were chosen to match those previously mapped by SCUBA-2, HARP, and *Herschel* in the JCMT and *Herschel* Gould Belt Surveys (Ward-Thompson et al. 2007; André et al. 2010).

3. Observations

SCUBA-2 is an innovative 10,000-pixel submillimeter camera (Holland et al. 2006) that has revolutionized submillimeter astronomy in terms of its ability to carry out wide-field surveys to previously unprecedented depths (e.g., Buckle et al. 2015; Pattle et al. 2015). SCUBA-2 uses transition-edge superconducting bolometer arrays, which come complete with in-focal-plane superconducting quantum interference device amplifiers and multiplexed readouts, and are cooled to 100 mK by a liquid-cryogen-free dilution refrigerator (Holland et al. 2006). It has two arrays that operate simultaneously in parallel, one with filters centered at 850 μm and one at 450 μm. In this paper we discuss 850 μm data only.

The polarimeter POL-2 (Bastien et al. 2005a, 2005b; P. Bastien et al. 2017, in preparation; Friberg et al. 2016) has an achromatic continuously rotating half-wave plate in order to modulate the signal at a faster rate (2 Hz) than atmospheric transparency fluctuations. This modulation significantly improves the reliability and accuracy of submillimeter polarimetric measurements. The signal is analyzed by a wire-grid polarizer. For calibration, a removable polarizer is also available.

Figure 1 shows a schematic of a rotating half-wave plate polarimeter, such as the POL-2 instrument. POL-2 has three optical components, which are (in the order that the radiation encounters them): the calibration polarizer (not shown in Figure 1), the rotating half-wave plate, and the polarizer. The components are mounted in a box fixed in front of the entrance window of the main cryostat of SCUBA-2. All components are mounted so that they can be taken in and out of the beam remotely, making it very easy and fast to start polarimetry at
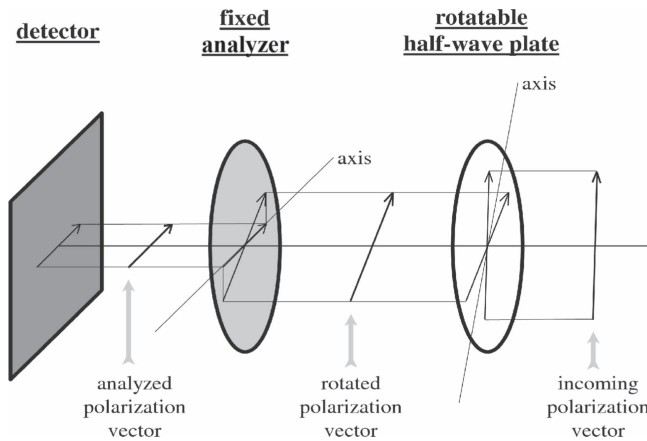
Figure 1. Schematic of a rotating half-wave plate polarimeter from Greaves et al. (2003).

Figure 2. Mean measured rms noise in Q and U as a function of time (in minutes) at a single off-source position. The data points show the scatter on the individual measurements, and the line is the running mean. A behavior consistent with $t^{-0.5}$ is seen, as in the ideal case.

the telescope (Bastien et al. 2005a, 2005b; P. Bastien et al. 2017, in preparation; Friberg et al. 2016).

The BISTRO time was allocated to take place during Band 2 weather ($0.05 < \tau_{225\,\mathrm{GHz}} < 0.08$), which is typical of moderately good weather conditions on Maunakea. The first data were taken with POL-2 on SCUBA-2 on 2016 January 11.

The POL-2 polarimeter fully samples circular regions with 12 arcmin diameter at a resolution of 14.1 arcsec in a version of the SCUBA-2 DAISY mapping mode (Holland et al. 2013) optimized for POL-2 observations (Friberg et al. 2016). The POL-2 DAISY scan pattern produces a central region of 3 arcmin diameter of approximately even coverage with high signal-to-noise ratio, with noise increasing to the edge of the map. The POL-2 DAISY scan pattern has a scan speed of 8 arcsec/s, with a half-wave plate rotation speed of 2 Hz (Friberg et al. 2016). Continuum observations are simulta-neously taken at 450 μm with a resolution of 9.6 arcsec, but as the 450 μm POL-2 observing mode has not yet been fully commissioned, we do not use these data in this paper.

The data were reduced in a two-stage process. The raw bolometer time-streams were first converted into separate Stokes Q and Stokes U time-streams using the process *calcqu* in SMURF (Chapin et al. 2013). The Q and U time-streams were then reduced separately using an iterative map-making technique, *makemap* in SMURF (Chapin et al. 2013), and gridded to 4 arcsec pixels. The iterations were halted when the map pixels, on average, changed by ⩽5% of the estimated map rms noise. In order to correct for the instrumental polarization (IP), *makemap* is supplied with a total intensity image of the source, taken using SCUBA-2 while POL-2 is not in the beam. The IP correction is discussed in detail by P. Bastien et al. (2017, in preparation). The total intensity image of OMC 1 presented in this paper was taken using the standard SCUBA-2 DAISY observing mode, and reduced using *makemap* using the same convergence criterion and pixel size as the POL-2 data.

The reduced scans were combined in two stages: (1) each of the Stokes Q observations were coadded to form a mosaic Stokes Q image (the Stokes U maps were coadded similarly); (2) each of the Stokes Q and U observations was combined using the process *pol2stack* in SMURF (Chapin et al. 2013) to produce an output half-vector catalog. We refer to data
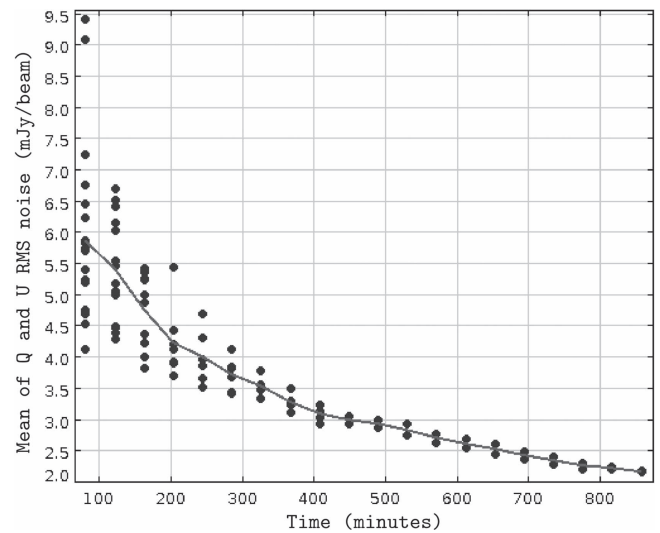
produced by these methods as BISTRO Internal Release 1 (IR1).

The data were calibrated in Jy/beam, using an aperture flux conversion factor (FCF) of 725 mJy/pW at 850 μm. When observing with POL-2, the standard SCUBA-2 850 μm FCF, of 537 Jy/beam, derived from average values of JCMT calibrators (Dempsey et al. 2013), is increased by a factor of 1.35 through additional losses introduced by POL-2 (Friberg et al. 2016; P. Bastien et al. 2017, in preparation).

The OMC 1 region was observed 21 times between 2016 January 11 and 25 in a mixture of very dry weather (Band 1; $\tau_{225\,\mathrm{GHz}} \leqslant 0.05$) and dry weather (Band 2; $0.05 \leqslant \tau_{225\,\mathrm{GHz}} \leqslant 0.08$) under JCMT project reference numbers M16AL004 (BISTRO) and M15BEC02 (POL-2 commissioning).

In order to determine the behavior of rms noise in our observations as a function of integration time, we measured the standard deviation on the Stokes Q and Stokes U values in a region with relatively constant signal in both the Stokes Q and the Stokes U maps, located between OMC 1 and the Orion Bar. This region, centered at approximately $05^{\mathrm{h}}35^{\mathrm{m}}21^{\mathrm{s}}$ $-05°23'36''$, was chosen because it was relatively flat, moderately unpolarized, low in emission, and away from the brightest sources, and because there was no region entirely without signal in the central part of the map. Figure 2 shows how the noise integrates down in this 21-repeat ($\sim$14 hr) POL-2 observation.

The polarization noise in Figure 2 is seen to integrate down close to $t^{-0.5}$, as in the ideal case. The scatter of individual measurements reduces satisfactorily as the data are subse-quently combined. We find that there is no evidence of any "noise floor" in long integrations. From this plot we see that this data set has reached 2.1 mJy beam^{-1} rms noise in 13.5 hr. An rms noise value of $\sim$2 mJy beam^{-1} was set as the target value for the BISTRO survey. Appendices A and B list a series of tests that we carried out to confirm the repeatability of our measurements and to demonstrate consistency with pre-vious data.
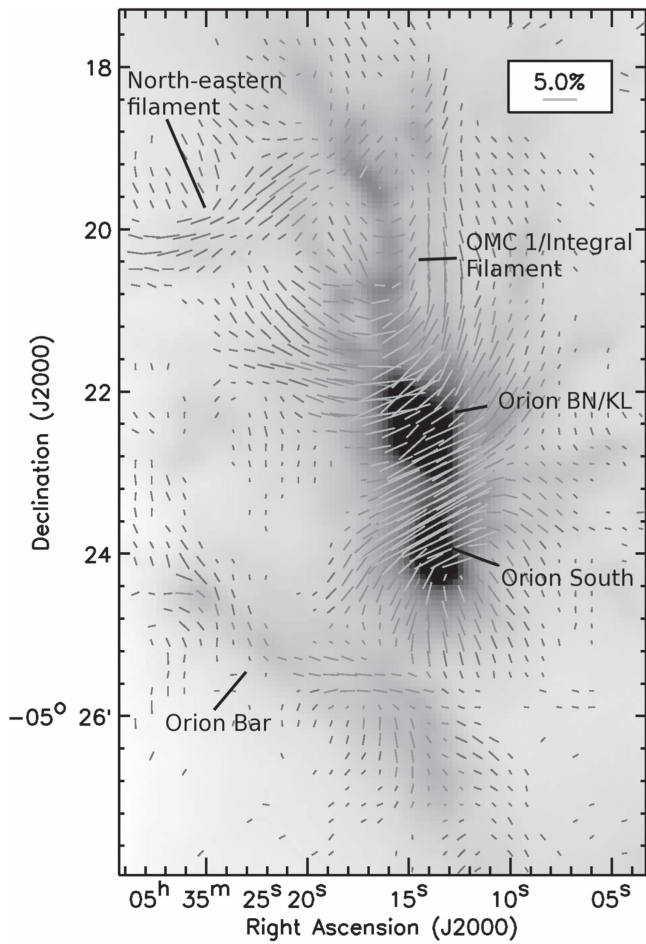
Figure 3. Polarization map of the OMC 1 region of the "integral filament" in Orion A, with half-vectors rotated by 90° to show the B-field direction. The Orion Bar can be seen in the southeastern part of the map. Half-vectors with $P/DP \geqslant 3$ are shown. The background image is a SCUBA-2 850 μm emission map taken using the standard SCUBA-2 DAISY mapping mode. The half-vector gray-scale is chosen for contrast against the background SCUBA-2 map.

4. First Data from the Survey

Figure 3 shows a polarization map taken with POL-2 of the OMC 1 region of the "integral filament" in the Orion A molecular cloud, with half-vectors rotated by 90° to trace the B-field direction. Only vectors with a signal-to-noise ratio of 3 or greater in polarization fraction are shown (i.e., $P/DP \geqslant 3$). The Orion A molecular cloud is a well-resolved and well-studied region of high-mass star formation (e.g., Bally 2008; O'Dell et al. 2008). It is the closest region of high-mass star formation, located at a distance of $388 \pm 5\,\mathrm{pc}$ (Kounkel et al. 2017). The half-vector lengths show the percentage polarization, with a 5% scale bar in the corner to give the calibration. The underlying image is an 850 μm total intensity map of the same region taken using SCUBA-2.

The "integral filament" (Bally et al. 1987) can be seen running roughly north-south through the region. The brightest part of the filament lies just south of the center of the image. The two brightest and most massive regions in the filament are the northern Becklin-Neugebauer Kleinmann-Low (BN/KL) object (Becklin & Neugebauer 1967; Kleinmann & Low 1967) and the southern Orion South clump (Batrla et al. 1983; Haschick & Baan 1989). Both are seen in Figure 3. In the

southeast part of the map the Orion Bar photon-dominated region (PDR) extends from the center of the foot of the map in a roughly northeasterly direction.

In the brightest central part of the filament, the B-field direction, as indicated by the half-vectors, appears to lie roughly orthogonal to the main axis of the filament. This pattern continues on the main axis line of the filament over most of the length of the filament. More particularly, on the brightest part of the filament the orientation of the long axis of the filament is estimated to be $+11^\circ.0 \pm 1^\circ.5$, while the calculated B-field direction is $-64^\circ.2 \pm 6^\circ.5$ (both measured north through east; note that there is a 180° ambiguity on the B-field direction), yielding a difference of $75^\circ.2 \pm 6^\circ.7$. The filament direction was estimated by performing a linear regression on the coordinates of 12 bright peaks of sub-millimeter emission located along the linear portion of the integral filament, as observed in the JCMT GBS 850 μm SCUBA-2 data. The field direction was estimated by taking the mean of the position angles of the B-field half-vectors in the region of uniform field direction in the center of the OMC 1 region, between the Orion BN/KL and S clumps.

However, away from the central axis of the filament, the field appears to curve to either side. In the northern half of the filament, the field appears to curve northward, delineating a rough U-shape, centered on the filament. In the southern half of the filament, the field appears to curve to the south, forming an inverted U-shape. This so-called "hourglass" morphology was first noted by Schleuning (1998) at much lower resolution and signal-to-noise ratio, observing at 100 and 350 μm with the Kuiper Airborne Observatory (KAO) and the Caltech Sub-millimeter Observatory, respectively. However, we note a far higher degree of curvature of the field lines than was seen by Schleuning (1998).

There is a slight degree of depolarization visible toward the centers of the BN-KL and Orion-S clumps. This is a well-known effect resulting from tangled fields in the centers of very dense regions (e.g., Matthews & Wilson 2002). The pattern along the Orion Bar appears somewhat more complex. Furthermore, in the northeastern section of the map there is a region of half-vectors that appear to follow a different pattern. Here the half-vectors seem to be running along a different filament. All of the above is consistent with the much lower signal-to-noise ratio data of Houde et al. (2004) and Matthews et al. (2009). The interferometry data of Rao et al. (1998) on the peaks of OMC 1 are also consistent with our data. We now discuss all of these features.

5. Discussion

Herschel has shown that the dominant formation mechanism for prestellar cores is core formation along filaments (André et al. 2014), revealing several examples of large-scale filaments lying perpendicular to the (plane-of-sky) B-field directions, as measured with large-scale absorption polarimetry (e.g., Palmeirim et al. 2013). This is consistent with findings from previous emission polarization measurements from SCUPOL on SCUBA (e.g., Matthews et al. 2001) and more recent large-scale polarization emission data from BLASTPol (e.g. Matthews et al. 2014). Based on these examples, a model has emerged whereby collapse occurs first along field lines to form filaments, and then along filaments to form cores (André et al. 2014). In the lower-density regions around the main
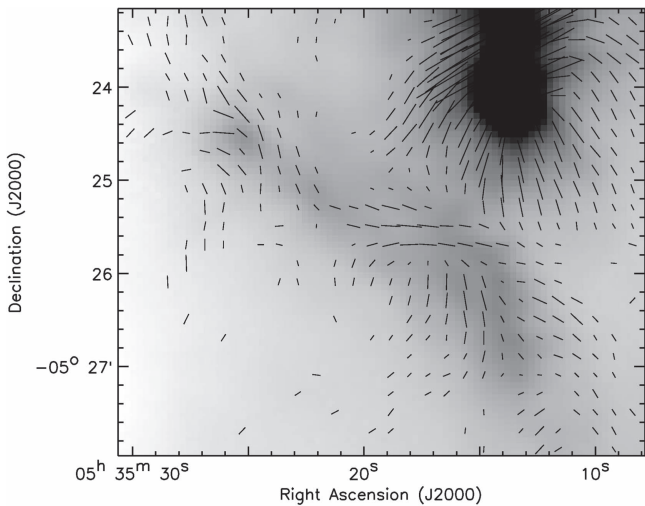
Figure 4. Polarization structure of the Orion Bar as observed with POL-2, with half-vectors rotated 90° to show the B-field direction.

filament, striations (or subfilaments) are typically seen parallel to the B-field (Palmeirim et al. 2013).

The polarization pattern we have observed in OMC 1 in Figure 3 follows this theoretical picture on-axis. The main part of the integral filament containing the BN-KL object and Orion South has a B-field direction apparently roughly orthogonal to the main filament direction, as mentioned above.

However, our wide-field data also allow us to trace the B-field direction off-axis, and it is here that even more interesting behavior is seen, as noted above, with a roughly "hourglass" morphology. If we follow this theoretical picture, then we would predict that the field lines started out roughly orthogonal to the filament in the lower density as well as the higher-density material, in a more uniform configuration, and was subsequently distorted into its current configuration.

There appear to be two possibilities as to how the hourglass morphology could have formed. One possibility is that the motion of the denser central material along the filament axis pulled the B-field lines into this configuration, as predicted by the model (see Figure 9(a) of André et al. 2014). Another possibility is that the well-known BN-KL outflow (Thaddeus et al. 1972) caused the field lines in the lower-density peripheral material to deviate from their original orientation. The effect of the highly collimated central part of the BN-KL outflow on the B-field on arcsecond scales is discussed by Tang et al. (2010).

We note that the outflow has a wide opening angle and high-velocity wings with multiple ejecta, often referred to as the "bullets of Orion" (Allen & Burton 1993). The central point of the outflow coincides with the position of the BN-KL object, the northern submillimeter-bright region in Figure 3. Consequently, the position and opening angle of the outflow roughly match the central part of the hourglass pattern, as well as the angle between the U-shape and the inverted U-shape fields, as if the outflow had pushed aside the field. Further work is required to decide which of these scenarios is correct.

A close-up of the Orion Bar region is shown in Figure 4. Here we see that the field follows a more complex morphology. At the southern end of the Bar, the field appears to be running north-south. In the middle of the Bar, the field runs roughly east-west. In the northern part of the Bar, the field appears to turn again to run in a northeasterly direction.
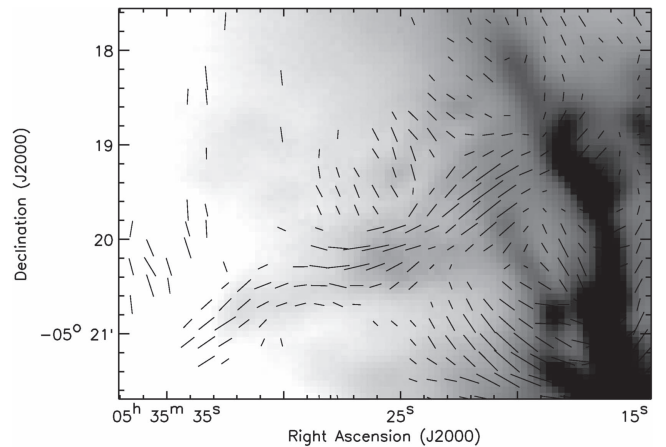

Figure 5. Polarization structure of the northeastern filament as observed with POL-2, with half-vectors rotated 90° to show the B-field direction.

This complex pattern clearly indicates a complex field structure. One possibility is a field that is simply twisting along the PDR front. Close examination of the Bar does appear to show that the Bar roughly twists in line with the field direction. Another possibility is that the field is running helically around the Orion Bar. In cases as complex as this, it is often difficult to determine which of a number of different three-dimensional scenarios is being projected onto our two-dimensional field of view (see, e.g., Franzmann & Fiege 2017). However, the simulations produced by Franzmann & Fiege (2017) show that a helical field could produce the polarization pattern that we are seeing.

Figure 5 shows a close-up of the northeastern filament that runs in a roughly east-west direction and is roughly orthogonal to the main integral filament. This is reminiscent of the subfilaments, or striations, seen in Taurus (Palmeirim et al. 2013), which lie perpendicular to the main filament. Figure 5 shows that the B-field lies roughly parallel to this subfilament, again as seen in Taurus (Palmeirim et al. 2013). Similar behavior is also seen in the low-density striations in the Polaris Flare region (Ward-Thompson et al. 2010; Panopoulou et al. 2016).

Furthermore, the B-field pattern lying along the northeastern filament appears to lie in the foreground relative to the hourglass field. Both north and south of the northeastern filament the field lies in a direction running northeast-southwest, as if it continued behind the northeastern filament. Hence, we hypothesize that the northeastern filament is foreground to the rest of the cloud.

This behavior of parallel versus perpendicular field geometries is predicted theoretically. For example, numerous studies of non-self-gravitating (i.e., low-density) filaments see B-fields lying parallel to filaments—essentially by running simulations without gravity (e.g., Heitsch et al. 2001; Ostriker et al. 2001; Falceta-Gonçalves et al. 2008). Nakamura & Li (2008) include self-gravity and see "elongated condensations (i.e., dense filaments) that are generally perpendicular to the large-scale field".

More recently, Soler et al. (2013) studied in detail the effects of varying the B-field strength in a filament, as well as varying the density of the filament. They found that field lines are preferentially perpendicular to the filaments above a certain critical density and parallel to the filaments below this density.

This is exactly what we see here—the field is running parallel to the low-density northeastern filament, and perpendicular to the high-density integral filament (see Figure 1 of Soler et al. 2013). Incidentally, Soler et al. (2013) find field lines perpendicular to filaments only in intermediate-strength and high-strength field cases. This would tend to indicate that the field we are observing in Orion is relatively strong.

6. Summary

In this paper we have introduced the BISTRO survey, which will map the dense regions of many nearby star-forming clouds with the POL-2 polarimeter and SCUBA-2 on the JCMT. We have described the rationale behind the survey, and the scientific questions that the survey will answer. The most important of these is the role of B-fields in the star formation process on small scales and in dense regions, and its importance relative to other processes, such as turbulent or nonthermal motions of the gas.

We have described the data acquisition and reduction processes for POL-2, demonstrating that the rms noise on BISTRO POL-2 observations decreases as $t^{-0.5}$, as expected. We presented the first POL-2 polarization map from the BISTRO survey, which is of the OMC 1 region of Orion A, and showed compatibility with previous observations, as well as repeatability of the POL-2 results.

We saw that the field lies perpendicular to the integral filament in the densest regions of that filament. Furthermore, we saw an hourglass B-field morphology extending beyond the densest region of the integral filament into the less-dense surrounding material, and discussed possible causes for this. We observed a more complex morphology along the Orion Bar.

We examined the morphology of the field along the lower-density northeastern filament. We found consistency with previous theoretical models that predict B-fields lying parallel to low-density, non-self-gravitating filaments, and perpendicular to higher-density, self-gravitating filaments.

Appendix A
Repeatability of POL-2 Observations

In this appendix we present a demonstration of the repeatability of POL-2 observations of extended structure. These results are a subset of a larger study to be presented in the POL-2 commissioning paper (P. Bastien et al. 2017, in preparation), to which we refer the reader for further information.

In order to test the repeatability of our observations, we performed jackknife tests on our observations of OMC 1. We divided the data into odd- and even-numbered scans, the half-vector maps produced from which are shown in Figure 6. This division of scans is intentionally arbitrary, and is used to show the variation that might be expected between any two samples, uncorrelated in any observational property. We see excellent consistency between the two maps.

Appendix B
Comparability of POL-2 to Previous Observations

In this appendix we compare the POL-2 map of OMC 1 to previous observations of OMC 1 made using the previous JCMT polarimeter, SCUPOL. There is no a priori reason to expect identical performance from SCUPOL and POL-2; the two instruments were/are mounted on different cameras (SCUBA and SCUBA-2 respectively; see Holland et al. 1999; Holland et al. 2006), and take data in different modes (see Greaves et al. 2003; Friberg et al. 2016; P. Bastien et al. 2017, in preparation). However, the two instruments take data at the same wavelength and resolution, and so the data taken ought to be directly comparable.

The SCUPOL observations of OMC 1 were published as part of the SCUPOL Legacy Catalog (Matthews et al. 2009). Figure 7 shows the SCUPOL data superposed on the POL-2 data. It can be seen that the POL-2 and SCUPOL half-vectors show a very similar morphology, but that the polarization fractions seen in the SCUPOL half-vectors are slightly larger than the POL-2 half-vectors. We believe that this is due to the lower signal-to-noise ratio of the older SCUPOL data.

The similarity in the polarization angles of the POL-2 and SCUPOL half-vectors is shown quantitatively in Figure 8. The
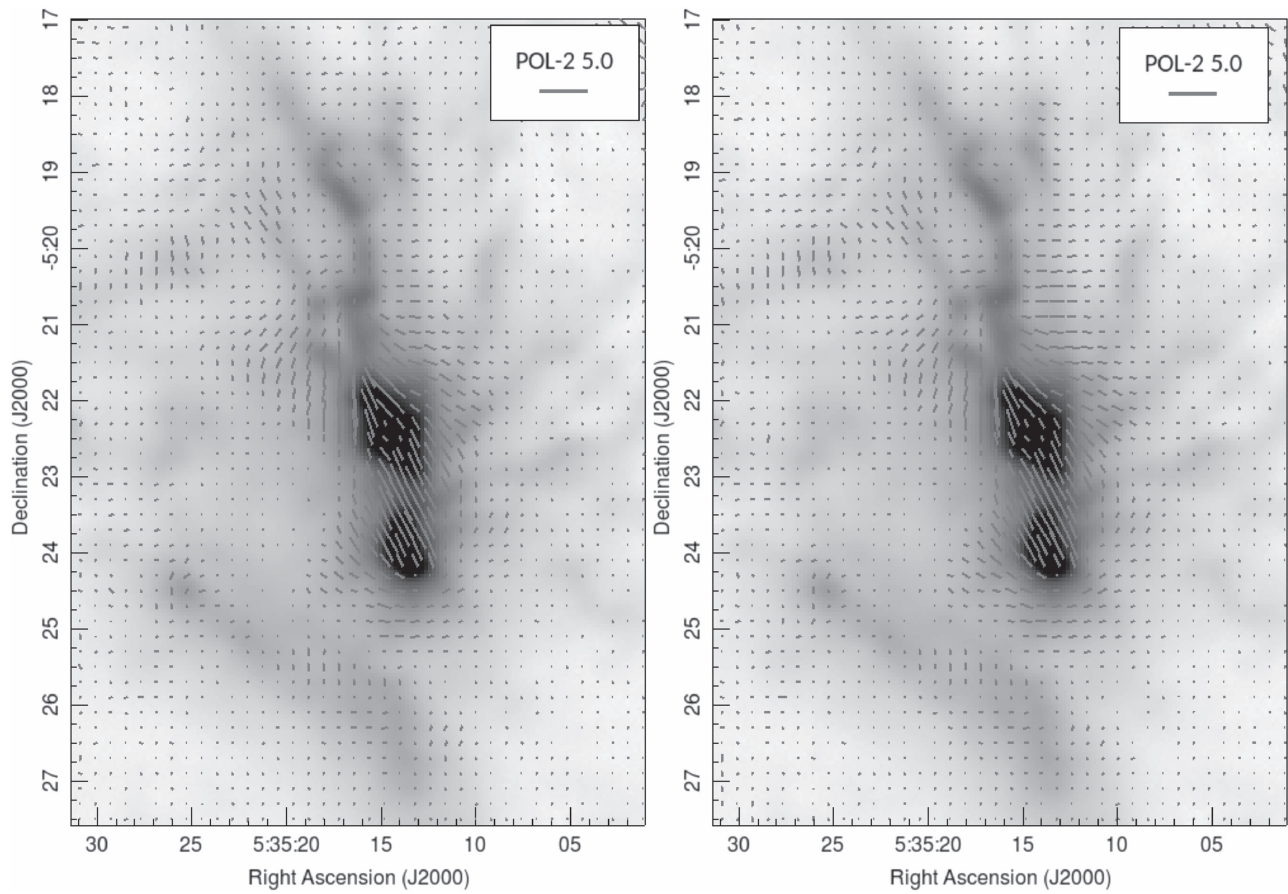
Figure 6. Jackknife test: polarization maps of the OMC 1 region of Orion A made from odd-numbered scans (left) and even-numbered scans (right). Note that here the half-vectors have not been rotated.
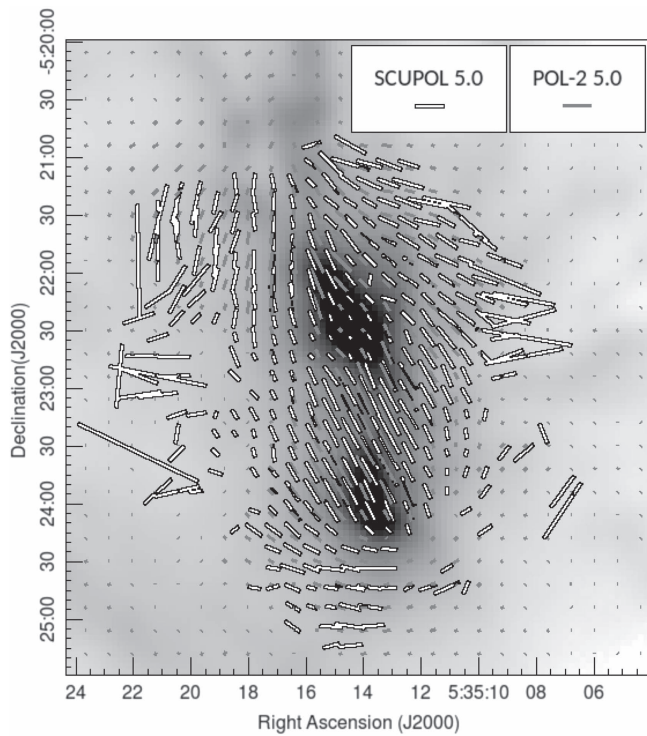

Figure 7. POL-2 (gray) and SCUPOL (white) half-vectors, overlaid on the JCMT GBS SCUBA-2 image of OMC 1.
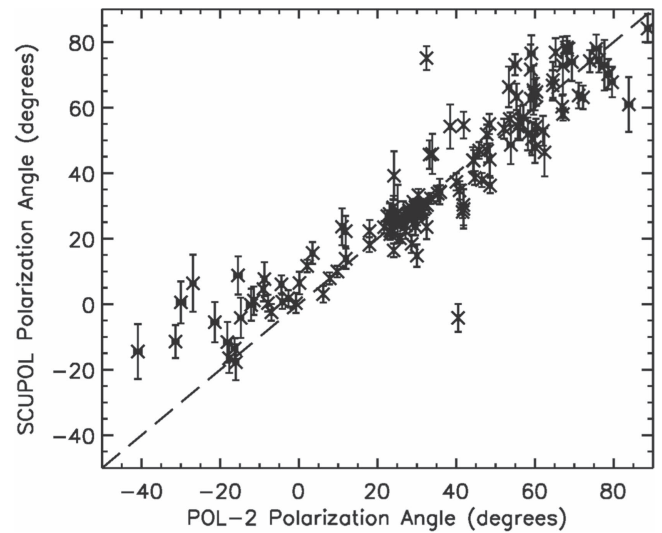

Figure 8. Polarization angles at matched coordinates in the POL-2 and SCUPOL maps. The dashed line shows the 1:1 line.

POL-2 and SCUPOL polarization angles are plotted at positions matched to within one JCMT beam (14.1 arcsec). The two half-vector sets show correlated polarization angles, and in fact the POL-2 and SCUPOL polarization angles are consistent with a 1:1 relationship.

References

Allen, D. A., & Burton, M. G. 1993, Natur, 363, 54

André, P., Di Francesco, J., Ward-Thompson, D., et al. 2014, in Protostars and Planets VI, ed. H. Beuther et al. (Tucson, AZ: Arizona Press), 27

André, P., Men'shchikov, A., Bontemps, S., et al. 2010, A&A, 518, L102

Bally, J. 2008, in Handbook of Star Forming Regions, Volume I: The Northern Sky, ed. B. Reipurth (San Francisco, CA: ASP), 459

Bally, J., Langer, W. D., Stark, A. A., & Wilson, R. W. 1987, ApJL, 312, L45

Balsara, D., Ward-Thompson, D., & Crutcher, R. M. 2001, MNRAS, 327, 715

Bastien, P., Bissonnette, É., Ade, P., et al. 2005a, JRASC, 99, 133

Bastien, P., Jenness, T., & Molnar, J. 2005b, in ASP Conf. Ser. 343, Astronomical Polarimetry: Current Status and Future Directions, ed. A. Adamson et al. (San Francisco, CA: ASP), 69

Basu, S., Ciolek, G. E., Dapp, W. B., & Wurster, J. 2009, NewA, 14, 483

Batrla, W., Wilson, T. L., Ruf, K., & Bastien, P. 1983, A&A, 128, 279

Becklin, E. E., & Neugebauer, G. 1967, ApJ, 147, 799

Berry, D. S., Gledhill, T. M., Greaves, J. S., & Jenness, T. 2005, in ASP Conf. Ser. 343, Astronomical Polarimetry: Current Status and Future Directions, ed. A. Adamson et al. (San Francisco, CA: ASP), 71

Buckle, J. V., Curtis, E. I., Roberts, J. F., et al. 2010, MNRAS, 401, 204

Buckle, J. V., Drabek-Maunder, E., Greaves, J., et al. 2015, MNRAS, 449, 2472

Burge, C. A., Van Loo, S., Falle, S. A. E. G., & Hartquist, T. W. 2016, A&A, 596, A28

Chandrasekhar, S., & Fermi, E. 1953, ApJ, 118, 113

Chapin, E. L., Berry, D. S., Gibb, A. G., et al. 2013, MNRAS, 430, 2545

Chapman, N. L., Davidson, J. A., Goldsmith, P. F., et al. 2013, ApJ, 770, 151

Chen, H.-R., Rao, R., Wilner, D. J., & Liu, S.-Y. 2012, ApJL, 751, L13

Chen, M. C.-Y., Di Francesco, J., Johnstone, D., et al. 2016, ApJ, 826, 95

Cho, J., & Lazarian, A. 2007, ApJ, 669, 1085

Cho, J., & Yoo, H. 2016, ApJ, 821, 21

Cortes, P. C., Girart, J. M., Hull, C. L. H., et al. 2016, ApJL, 825, L15

Crutcher, R. M. 2012, ARA&A, 50, 29

Crutcher, R. M., Nutter, D. J., Ward-Thompson, D., & Kirk, J. M. 2004, ApJ, 600, 279

Crutcher, R. M., Troland, T. H., Lazareff, B., & Kazes, I. 1996, ApJ, 456, 217

Crutcher, R. M., Wandelt, B., Heiles, C., Falgarone, E., & Troland, T. H. 2010, ApJ, 725, 466

Currie, M. J., Berry, D. S., Jenness, T., et al. 2014, in ASP Conf. Ser. 485, Astronomical Data Analysis Software and Systems XXIII, ed. N. Manset & P. Forshay (San Francisco, CA: ASP), 39

Dempsey, J. T., Friberg, P., Jenness, T., et al. 2013, MNRAS, 430, 2534

Dotson, J. L., Vaillancourt, J. E., Kirby, L., et al. 2010, ApJS, 186, 406

Falceta-Gonçalves, D., Lazarian, A., & Kowal, G. 2008, ApJ, 679, 537

Fiege, J. D., & Pudritz, R. E. 2000a, MNRAS, 311, 85

Fiege, J. D., & Pudritz, R. E. 2000b, MNRAS, 311, 105

Fissel, L. M. 2015, IAUGA, 22, 2257545

Fissel, L. M., Ade, P. A. R., Angilè, F. E., et al. 2016, ApJ, 824, 134

Franzmann, E. L., & Fiege, J. D. 2017, MNRAS, 466, 4592

Friberg, P., Bastien, P., Berry, D., et al. 2016, Proc. SPIE, 9914, 991403

Galli, D., & Shu, F. H. 1993, ApJ, 417, 220

Girart, J. M., Rao, R., & Marrone, D. P. 2006, Sci, 313, 812

Goodman, A. A., Bastien, P., Menard, F., & Myers, P. C. 1990, ApJ, 359, 363

Graves, S. F., Richer, J. S., Buckle, J. V., et al. 2010, MNRAS, 409, 1412

Greaves, J. S., Holland, W. S., Jenness, T., et al. 2003, MNRAS, 340, 353

Haschick, A. D., & Baan, W. A. 1989, ApJ, 339, 949

Heitsch, F., Naab, T., & Walch, S. 2011, MNRAS, 415, 271

Heitsch, F., Zweibel, E. G., Mac Low, M.-M., Li, P., & Norman, M. L. 2001, ApJ, 561, 800

Hennebelle, P., & Fromang, S. 2008, A&A, 477, 9

Hennebelle, P., & Teyssier, R. 2008, A&A, 477, 25

Hildebrand, R. H., Kirby, L., Dotson, J. L., Houde, M., & Vaillancourt, J. E. 2009, ApJ, 696, 567

Holland, W., MacIntosh, M., Fairley, A., et al. 2006, Proc. SPIE, 6275, 62751E

Holland, W. S., Bintley, D., Chapin, E. L., et al. 2013, MNRAS, 430, 2513

Holland, W. S., Robson, E. I., Gear, W. K., et al. 1999, MNRAS, 303, 659

Houde, M., Dowell, C. D., Hildebrand, R. H., et al. 2004, ApJ, 604, 717

Houde, M., Hezareh, T., Jones, S., & Rajabi, F. 2013, ApJ, 764, 24

Houde, M., Vaillancourt, J. E., Hildebrand, R. H., Chitsazzadeh, S., & Kirby, L. 2009, ApJ, 706, 1504

Hull, C. L. H., Plambeck, R. L., Bolatto, A. D., et al. 2013, ApJ, 768, 159

Hull, C. L. H., Plambeck, R. L., Kwon, W., et al. 2014, ApJS, 213, 13

Inoue, T., & Inutsuka, S.-i. 2008, ApJ, 687, 303

Inoue, T., & Inutsuka, S.-i. 2009, ApJ, 704, 161

Inoue, T., & Inutsuka, S.-i. 2012, ApJ, 759, 35

Inutsuka, S.-i., Inoue, T., Iwasaki, K., & Hosokawa, T. 2015, A&A, 580, A49

Kirk, H., Di Francesco, J., Johnstone, D., et al. 2016, ApJ, 817, 167

Kirk, J. M., Ward-Thompson, D., & Crutcher, R. M. 2006, MNRAS, 369, 1445

Kleinmann, D. E., & Low, F. J. 1967, ApJL, 149, L1

Klessen, R. S., Heitsch, F., & Mac Low, M.-M. 2000, ApJ, 535, 887

Kounkel, M., Hartmann, L., Loinard, L., et al. 2017, ApJ, 834, 142

Kwon, J., Tamura, M., Hough, J. H., et al. 2015, ApJS, 220, 17

Lazarian, A., & Hoang, T. 2008, ApJL, 676, L25

Li, H.-B., Goodman, A., Sridharan, T. K., et al. 2014, Protostars and Planets VI, 101

Li, Z.-Y., Krasnopolsky, R., & Shang, H. 2011, ApJ, 738, 180

Li, Z.-Y., & Nakamura, F. 2004, ApJL, 609, L83

Li, Z.-Y., Wang, P., Abel, T., & Nakamura, F. 2010, ApJL, 720, L26

Machida, M. N., Inutsuka, S.-I., & Matsumoto, T. 2011, PASJ, 63, 555

Machida, M. N., Matsumoto, T., Tomisaka, K., & Hanawa, T. 2005, MNRAS, 362, 369

Mac Low, M.-M., & Klessen, R. S. 2004, RvMP, 76, 125

Mairs, S., Johnstone, D., Kirk, H., et al. 2016, MNRAS, 461, 4022

Matthews, B. C., McPhee, C. A., Fissel, L. M., & Curran, R. L. 2009, ApJS, 182, 143

Matthews, B. C., & Wilson, C. D. 2002, ApJ, 574, 822

Matthews, B. C., Wilson, C. D., & Fiege, J. D. 2001, ApJ, 562, 400

Matthews, T. G., Ade, P. A. R., Angilè, F. E., et al. 2014, ApJ, 784, 116

Mouschovias, T. C. 1991, ApJ, 373, 169

Nagai, H., Nakanishi, K., Paladino, R., et al. 2016, ApJ, 824, 132

Nakamura, F., & Li, Z.-Y. 2005, ApJ, 631, 411

Nakamura, F., & Li, Z.-Y. 2008, ApJ, 687, 354

O'Dell, C. R., Muench, A., Smith, N., & Zapata, L. 2008, in Handbook of Star Forming Regions, Volume I: The Northern Sky, ed. B. Reipurth (San Francisco, CA: ASP), 544

Ostriker, E. C., Stone, J. M., & Gammie, C. F. 2001, ApJ, 546, 980

Padoan, P., & Nordlund, Å. 1999, ApJ, 526, 279

Padoan, P., & Nordlund, Å. 2002, ApJ, 576, 870

Palmeirim, P., André, P., Kirk, J., et al. 2013, A&A, 550, A38

Panopoulou, G. V., Psaradaki, I., & Tassis, K. 2016, MNRAS, 462, 1517

Pascale, E., Ade, P. A. R., Bock, J. J., et al. 2008, ApJ, 681, 400

Pattle, K., Ward-Thompson, D., Kirk, J. M., et al. 2015, MNRAS, 450, 1094

Pattle, K., Ward-Thompson, D., Kirk, J. M., et al. 2017, MNRAS, 464, 4255

Planck Collaboration, Ade, P. A. R., Aghanim, N., et al. 2015, A&A, 576, A104

Planck HFI Core Team, 2011, A&A, 536, A4

Price, D. J., & Bate, M. R. 2007, MNRAS, 377, 77

Rao, R., Crutcher, R. M., Plambeck, R. L., & Wright, M. C. H. 1998, ApJL, 502, L75

Richer, J. S., Padman, R., Ward-Thompson, D., Hills, R. E., & Harris, A. I. 1993, MNRAS, 262, 839

Rumble, D., Hatchell, J., Gutermuth, R. A., et al. 2015, MNRAS, 448, 1551

Sadavoy, S. I., Di Francesco, J., Johnstone, D., et al. 2013, ApJ, 767, 126

Salji, C. J., Richer, J. S., Buckle, J. V., et al. 2015, MNRAS, 449, 1769

Schleuning, D. A. 1998, ApJ, 493, 811

Segura-Cox, D. M., Looney, L. W., Stephens, I. W., et al. 2015, ApJL, 798, L2

Seifried, D., & Walch, S. 2015, MNRAS, 452, 2410

Shibata, K., & Matsumoto, R. 1991, Natur, 353, 633

Soler, J. D., Hennebelle, P., Martin, P. G., et al. 2013, ApJ, 774, 128

Sugitani, K., Nakamura, F., Watanabe, M., et al. 2011, ApJ, 734, 63

Tamura, M., & Kwon, J. 2015, in Polarimetry of Stars and Planetary Systems, ed. L. Kolokolova, J. Hough, & A.-C. Levasseur-Regourd (Cambridge: Cambridge Univ. Press), 162

Tang, Y.-W., Ho, P. T. P., Koch, P. M., & Rao, R. 2010, ApJ, 717, 1262

Thaddeus, P., Kutner, M. L., Penzias, A. A., Wilson, R. W., & Jefferts, K. B. 1972, ApJL, 176, L73

Tomisaka, K. 2015, ApJ, 807, 47

Troland, T. H., & Crutcher, R. M. 2008, ApJ, 680, 457

Vaillancourt, J. E., & Matthews, B. C. 2012, ApJS, 201, 13

Vázquez-Semadeni, E., Banerjee, R., Gómez, G. C., et al. 2011, MNRAS, 414, 2511

Ward-Thompson, D., Di Francesco, J., Hatchell, J., et al. 2007, PASP, 119, 855

Ward-Thompson, D., Kirk, J. M., André, P., et al. 2010, A&A, 518, L92

Ward-Thompson, D., Kirk, J. M., Crutcher, R. M., et al. 2000, ApJL, 537, L135

Ward-Thompson, D., Pattle, K., Kirk, J. M., et al. 2016, MNRAS, 463, 1008

Ward-Thompson, D., Sen, A. K., Kirk, J. M., & Nutter, D. 2009, MNRAS, 398, 394

White, G. J., Drabek-Maunder, E., Rosolowsky, E., et al. 2015, MNRAS, 447, 1996